the system to point R or L and thus exciting autonomous oscillations in one of the qubits (Fig. 3a). The spectra of the oscillations can be fitted to a cosine function with an exponential decay time of about 2.5 ns. The spectra of the oscillations (right panels of Fig. 3a) obtained by Fourier transform contain one pronounced component at 13.4 GHz for the first qubit and at 9.1 GHz for the second qubit. We identify these values with E_{J1} and E_{J2}. Judging from our previous experiments (see, for example, ref. 13) we conclude that these values are close to what we expect for the given fabrication parameters (that is, overlap area and oxidation conditions). Then, by changing n_{g1} and n_{g2}, the system is driven to the co-resonance point, and the induced quantum oscillations are traced using the same technique. The oscillation pattern becomes more complex (Fig. 3b), and more frequency components appear in the spectrum. The observed spectral properties of the oscillations agree with the predictions of equation (3), in that there are two peaks in the spectrum and the peak positions are close to the expected frequencies $\Omega + \varepsilon$ and $\Omega - \varepsilon$ for the parameters $E_{J1} = 13.4\,\mathrm{GHz}$ and $E_{J2} = 9.1\,\mathrm{GHz}$ measured in the single qubit experiments (Fig. 3a), and $E_m = 15.7\,\mathrm{GHz}$ estimated from independent measurements of d.c. current–voltage–gate-voltage characteristics. The positions of the $\Omega + \varepsilon$ and $\Omega - \varepsilon$ peaks expected from equation (3) are indicated by arrows and dotted lines in Fig. 3. The decay time ($\sim$0.6 ns) of the coupled oscillations is shorter compared to the case of the independent oscillations, as is expected because an extra decoherence channel appears for each qubit after coupling it to its neighbour. However, the amplitudes of the spectral peaks do not exactly agree with equation (3). We attribute this to the non-ideal pulse shape (finite rise/fall time $\sim$35 ps), and the fact that a small shift of n_{g1} and n_{g2} off the co-resonance drastically changes the oscillation pattern. Also, even far from the co-resonance, we still have a small contribution to the initial state from charge states other than $|00\rangle$ distorting the oscillations. We have performed numerical simulations of the oscillation pattern, taking into account a realistic pulse shape and an initial condition of not pure $|00\rangle$, assuming the system is exactly at the co-resonance. The resulting fits are shown in Fig. 3b as solid lines. We found that $E_m = 14.5\,\mathrm{GHz}$, close to the value estimated from the d.c. measurements, gives better agreement of the fit with the experimental data.

Finally, we checked the dependence of the oscillation frequencies on E_{J1}, controlled by a weak magnetic field (up to 20 G). The results are shown in Fig. 4. The plot contains the data from both qubits represented by open triangles (first qubit) and open circles (second qubit). Without coupling ($E_m = 0$), the single peaks in each qubit would follow the dashed lines with an intersection at $E_{J1} = E_{J2}$. The introduced coupling modifies this dependence by creating a gap, and shifting the frequencies to higher and lower values; the spacing between the two branches is equal to $E_m/2h$ when $E_{J1} = E_{J2}$. We compare the observed dependence with the prediction of equation (3) (given by solid lines) and find a remarkable agreement.

The observed quantum coherent dynamics of coupled qubits in the vicinity of the co-resonance (in particular, the double-frequency structure of the probability oscillations in both qubits, and frequency 'repulsion' at $E_{J1} \approx E_{J2}$—see Figs 3b and 4) indicates that the two qubits become entangled during the course of coupled oscillations, although direct measurement of the degree of entanglement was not possible. Simple calculations based on the standard expression for the entanglement of the pure states[16] show that, with an ideal pulse shape and the $|00\rangle$ initial condition, the wavefunction shown in equation (2) evolves through a maximally entangled state in the case of equal Josephson energies. The numerical simulations confirm that the amount of entanglement does not decrease significantly when realistic experimental conditions are taken into account. The relatively large observed oscillation amplitude (about 50% of the expected value) also suggests the existence of entangled states even in our multi-pulse averaged experiment. □

Received 21 October; accepted 10 December 2002; doi:10.1038/nature01365.

1. Nielsen, M. A. & Chuang, I. L. *Quantum Computation and Quantum Information* (Cambridge Univ. Press, Cambridge, 2000).
2. Clark, R. G. (ed.) *Experimental Implementation of Quantum Computation* (Rinton, Princeton, 2001).
3. Averin, D. V. Quantum computing and quantum measurement with mesoscopic Josephson junctions. *Fortschr. Phys.* **48,** 1055–1074 (2000).
4. Makhlin, Y., Schön, G. & Shnirman, A. Quantum state engineering with Josephson-junction devices. *Rev. Mod. Phys.* **73,** 357–400 (2001).
5. Nakamura, Y., Pashkin, Yu. A. & Tsai, J. S. Coherent control of macroscopic quantum states in a single-Cooper-pair box. *Nature* **398,** 786–788 (1999).
6. Vion, D. *et al.* Manipulating the quantum state of an electrical circuit. *Science* **296,** 886–889 (2002).
7. Yu, Y., Han, S., Chu, X., Chu, S.-I. & Wang, Z. Coherent temporal oscillations of macroscopic quantum states in a Josephson junction. *Science* **296,** 889–892 (2002).
8. Martinis, J. M., Nam, S., Aumentado, J. & Urbina, C. Rabi oscillations in a large Josephson-junction qubit. *Phys. Rev. Lett* **89,** 117901 (2002).
9. Friedman, J. R., Patel, V., Chen, W., Toltygo, S. K. & Lukens, J. E. Quantum superposition of distinct macroscopic states. *Nature* **406,** 43–46 (2000).
10. Van der Wal, C. H. *et al.* Quantum superposition of macroscopic persistent-current states. *Science* **290,** 773–777 (2000).
11. Bouchiat, V., Vion, D., Joyez, P., Esteve, D. & Devoret, M. H. Quantum coherence with a single Cooper pair. *Phys. Scripta T* **76,** 165–170 (1998).
12. Flees, D. J., Han, S. & Lukens, J. E. Interband transitions and band gap measurements in Bloch transistors. *Phys. Rev. Lett.* **78,** 4817–4820 (1997).
13. Nakamura, Y., Chen, C. D. & Tsai, J. S. Spectroscopy of energy-level splitting between two macroscopic quantum states of charge coherently superposed by Josephson coupling. *Phys. Rev. Lett.* **79,** 2328–2331 (1997).
14. Esteve, D. in *Single Charge Tunneling* (eds Grabert, H. & Devoret, M. H.) 109–137 (Plenum, New York, 1992).
15. Fulton, T. A., Gammel, P. L., Bishop, D. J., Dunkleberger, L. N. & Dolan, G. J. Observation of combined Josephson and charging effects in small tunnel junction circuits. *Phys. Rev. Lett.* **63,** 1307–1310 (1989).
16. Bennett, C. H., Bernstein, H. J., Popescu, S. & Schumacher, B. Concentrating partial entanglement by local operations. *Phys. Rev. A* **53,** 2046–2052 (1996).

Acknowledgements We thank B. L. Altshuler, X. D. Hu, H. Im, S. Ishizaka, F. Nori, T. Sakamoto and J. Q. You for discussions. D.V.A. was supported by AFORS, and by NSA and ARDA under an ARO contract.

Competing interests statement The authors declare that they have no competing financial interests.

Correspondence and requests for materials should be addressed to J.S.T. (e-mail: tsai@frl.cl.nec.co.jp).

Probing molecular dynamics with attosecond resolution using correlated wave packet pairs

Hiromichi Niikura*, F. Légaré*†, R. Hasbani*, Misha Yu Ivanov*, D. M. Villeneuve* & P. B. Corkum*

** National Research Council of Canada, 100 Sussex Drive, Ottawa, Ontario K1A 0R6, Canada*
† Université de Sherbrooke, Sherbrooke PQ, Canada

Spectroscopic measurements with increasingly higher time resolution are generally thought to require increasingly shorter laser pulses, as illustrated by the recent monitoring of the decay of core-excited krypton[1] using attosecond photon pulses[2,3]. However, an alternative approach to probing ultrafast dynamic processes might be provided by entanglement, which has improved the precision[4,5] of quantum optical measurements. Here we use this approach to observe the motion of a D_2^+ vibrational wave packet formed during the multiphoton ionization of D_2 over several femtoseconds with a precision of about 200 attoseconds and 0.05 ångströms, by exploiting the correlation between the electronic and nuclear wave packets formed during the ionization event. An intense infrared laser field drives the electron wave packet, and electron recollision[6–11] probes the nuclear motion. Our results show that laser pulse duration need

not limit the time resolution of a spectroscopic measurement, provided the process studied involves the formation of correlated wave packets, one of which can be controlled; spatial resolution is likewise not limited to the focal spot size or laser wavelength.

Our experiment is analogous to conventional pump–probe measurements[12], but the pump and probe occur within one optical cycle, a process that we call 'sub-laser-cycle molecular dynamics' (Fig. 1a). Ionization, which forms correlated wave packets around each peak of the laser field, is the pump. By removing one electron (creating an electron wave packet in the continuum), we weaken the force binding the protons and therefore launch a correlated vibrational wave packet (Fig. 1b). Because of its small mass, only the electron wave packet is influenced by the laser field. In linear polarization, the electron wave packet is first moved away from the parent ion but is pulled back by the laser field. The probability of electron re-collision with the parent ion reaches a maximum at a well-defined laser phase, about two-thirds of an optical period after the electron's transition to the continuum (Fig. 1a). Re-collision probes the vibrational wave packet (Fig. 1b). Changing the laser wavelength delays re-collision just as changing the position of a translation stage changes an optical pump–probe delay. (Neither re-collision nor the pump–probe analogy is essential: fast measurements are possible in their absence if both correlated partners are controlled, as discussed below.)

Re-collision between an electron and its parent ion has long been known as a source of high-harmonics emission[7,8,13,14] and generation of high-energy electrons[7,9]. It is also responsible for correlated multi-electron ionization in strong laser fields[7,10,13], fragmentation in small molecules[11] and attosecond pulse generation[2,3,15]. For molecules, re-collision will also imprint the spatial structure of the ion on the harmonic emission spectrum[16] or on the photoelectron spectrum[6] in analogy with conventional electron diffraction (see, for example, ref. 17).

We use 40-fs laser pulses with an intensity of $1.5 \times 10^{14}\,\mathrm{W\,cm^{-2}}$ tunable from 800 to 1,850 nm. Ionization induces vertical population transfer from the D_2 ($X\,^1\Sigma_g^+$) potential energy surface to the D_2^+ ($X\,^2\Sigma_g^+$) surface, with less than 10^{-6} of the population transferred to any other levels of D_2^+ (I. Litvinyuk, P. Dooley, D.M.V. and P.B.C., manuscript in preparation). Because the equilibrium internuclear separation is greater for D_2^+ (1.06 Å) than for D_2 (0.74 Å), ionization initiates a vibrational wave packet motion (Fig. 1b). For all wavelengths that we use, the instantaneous ionization rate[18] is sharply peaked near the instantaneous maxima of the oscillating field. The ionization bursts last 190–300 as (800 nm to 1.85 μm). The nuclei are essentially frozen by their inertia on that timescale, ensuring that the pump stage is the same for all wavelengths.

We use electron–ion re-collision to observe motion on the D_2^+ ($X\,^2\Sigma_g^+$) surface. Although the electron returns to the parent ion

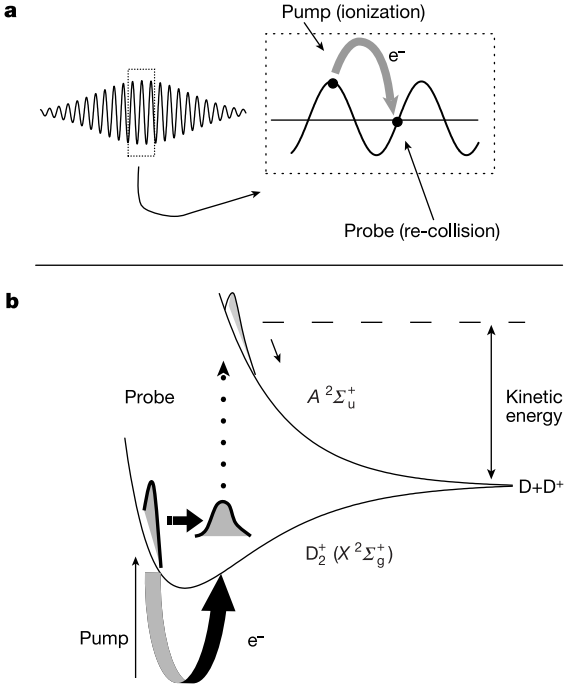

Figure 1 Processes probed and exploited with the sub-laser-cycle dynamics method using correlated wave packet pairs. **a**, Ionization forms correlated electronic and vibrational wave packets near each peak of the laser field. **b**, The vibrational wave packet moves on the D_2^+ ($X\,^2\Sigma_g^+$) surface while the laser field causes the electron wave packet to re-collide (represented by a thick arrow in **a** and **b**). Inelastic scattering during re-collision probes the vibrational wave packet's position. We measure the kinetic energy of the D^+ fragments (**b**).

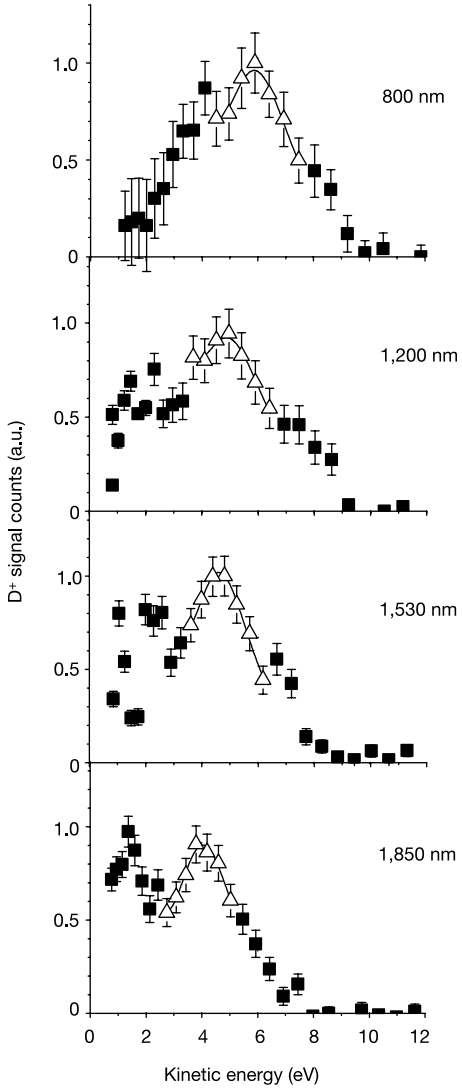

Figure 2 Kinetic energy distribution of D^+ at different pump–probe delay times. Shown is the experimental kinetic energy distribution of D^+ obtained using four different laser wavelengths, corresponding to different pump–probe delay times. Experimental error is estimated for each point by taking the square root of the signal counts. We identify the largest high-energy peak by the open data points with dissociation from D_2^+ ($A\,^2\Sigma_u^+$). The curve is obtained by a fit to the data as described in the text.

several times after ionization, the first return of the electron wave packet dominates[6] and can thus be used as a probe pulse with a duration of about 1 fs at 800 nm (ref. 6). The time delay between the creation of the correlated wave packets and their re-collision (pump–probe delay) is controlled by varying the laser wavelength. Our delay times range from 1.7 to 4.2 fs (about two-thirds of the period for $\lambda = 800$–1,850 nm).

Inelastic scattering of the electron with the parent ion leads to excitation or double ionization, giving rise to the dissociative fragments of D^+. The kinetic energy of the fragments is determined by the internuclear separation at the time of electron re-collision. By using a small aperture in the time-of-flight apparatus, we observe only those fragments that originate from molecules aligned perpendicular to the laser polarization. This configuration eliminates laser-induced coupling between $X\ ^2\Sigma_g^+$ and $A\ ^2\Sigma_u^+$. Our choice of alignment ensures that the wave packet motion is simple, that it can be easily modelled and that $A\ ^2\Sigma_u^+$ is a good reference state. The existence of the well-understood reference state allows us to unequivocally interpret the kinetic energy spectrum and use it to measure the position of the vibrational wave packet.

Figure 2 shows the kinetic energy spectrum of D^+ that is due to re-collision, for all wavelengths that we have studied. Although many dissociation pathways contribute to the observed kinetic energy spectra, we can isolate the Σ_u state as particularly significant. This is because, among all inelastic scattering events from the Σ_g surface, excitation to Σ_u has the highest cross-section over the energy range examined here[19]. In addition, the Σ_u leads to fragments with the second-largest kinetic energy. Therefore this channel is easily identified in Fig. 2. We have labelled the data points that we associate with this channel with triangles. In Fig. 2 we see the motion of the wave packet reflected in the shift of this peak to lower energy with longer wavelength light.

To convert the measured kinetic energy spectrum to the vibrational wave packet on the Σ_g surface, we use the reflection principle[20]. The transformation includes the radial dependence of the collision cross-section, and a self-consistent addition of the kinetic energy of the $D_2^+\ \Sigma_g^+$ wave packet, assuming that the initial average wave packet velocity is zero and initial average kinetic energy is given by the zero-point energy of D_2. We then fit the wave packet with a gaussian. Its projection back to the kinetic energy spectrum yields the solid curves in Fig. 2. The gaussian fit on Σ_g determines the experimentally measured wave packet and the position of its peak. We emphasize that this is a fit to the experimental data, not a theoretical curve.

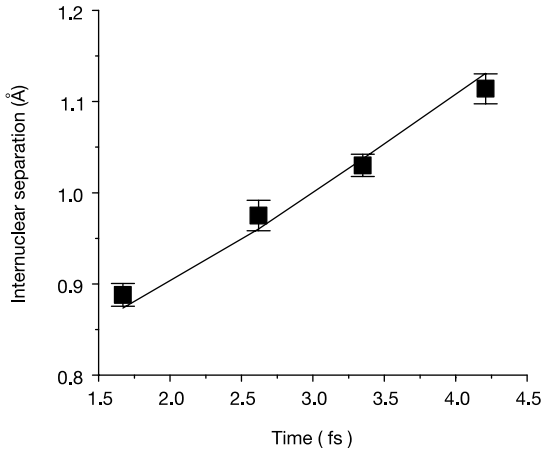

Figure 3 The measured wave packet position as a function of time. To associate the laser wavelength with the time of re-collision, we use the mean time of re-collision for the first electron micro-bunch at each laser wavelength. The position is determined from the peak of the fit in Fig. 2. The experimental error bars are determined by the error of the fit. The solid line is the calculated nuclear position as a function of time for a wave packet evolving on the D_2^+ ($X\ ^2\Sigma_g^+$) state. Because the time window that we measure is only about one-quarter of the full vibrational period of D_2^+ ($X\ ^2\Sigma_g^+$), the motion is almost linear.

Figure 3 is a plot of the experimentally determined internuclear separation as a function of time. We represent the position of the vibrational wave packet by the peak position of the gaussian at each laser wavelength. At each wavelength, the re-collision time is defined by the mean time for the electron wave packet's first return. This establishes the experimental points in Fig. 3. The error bars are determined by the deviation of the fit. We determine the position and the velocity of the wave packet with sub-fs, sub-Å resolution.

Because we are demonstrating a new technique for ultrafast measurement, it is important to compare our measurement against a standard. The solid line in Fig. 3 is the result of a simulation of the motion of a vibrational wave packet on the Σ_g surface by solving the time-dependent Schrödinger equation. The discrepancy is within the error bars.

The portion of the kinetic energy distribution that is higher than that assigned to the Σ_u state in Fig. 2 corresponds to transitions to the D_2^{++} state. For 800 nm the re-collision kinetic energy is insufficient to ionize D_2^+, but at other wavelengths a contribution can be seen. The peak at lower kinetic energy is not clearly identified. It contains contributions of other excited states and of the electron's multiple returns[6]. These are also seen to move to lower kinetic energies as the re-collision time is delayed.

Our current measurement accuracy is limited by noise, but noise in our data is not a fundamental limit. Using three-dimensional imaging detectors instead of observing through a small pinhole would increase our signal strength by about two orders of magnitude. A high-density jet source and a laser with higher repetition rate could further increase our signal by orders of magnitude.

Our method is based on the principle of creating two correlated wave packets that could be formed on any crest of the laser field. We assert that these wave packets are actually entangled. A field crest occurs once during each half-period throughout the 40-fs pulse. Unless the electron and vibrational wave packet are entangled, the kinetic energy spectrum for D^+ must have a 3-eV modulation (for 800 nm light, 1.5 eV per deuteron). Such modulation is well known in strong-field single-particle processes such as high harmonics generated by ionizing atomic media[8,9,13,14].

In fact, there is no 1.5 eV modulation in the kinetic energy spectrum at 800 nm in Fig. 2. We measured the spectrum with higher resolution to seek such modulation; none was observed. These experimental results are consistent with the vibrational and electron wave packets being entangled. Entanglement arises because the departing electron contains information on the nuclear coordinate at the time of ionization and on the excited state of the D_2^+ formed in the re-collision. By observing only the deuterium ions, we integrate over all final states of other unseen, but entangled, partner particles. Such partial measurement eliminates the interference.

Regarding future applications, we note that the ultimate time resolution of correlated measurements is determined by the energy bandwidth of the electron bunch—many tens of electron volts in the present experiment. To obtain a resolution of 200 as will be a challenge similar to that of producing the shortest optical pulses[2].

Also, as long as both particles can be controlled, re-collision is unnecessary. For example, if two electrons are ejected into a field in a correlated fashion, the time difference between their ejection is mapped onto the final energy and angular spectra[10,15,21].

Correlated particles produced in a process with important dynamics to probe can always be measured as long as at least one of the pair can be controlled. Because of their low mass, electrons are easily controlled, and at progressively higher intensitites, muons, protons, alpha particles and ions are also controllable. Applying correlation to nuclear dynamics requires a means of stimulating a process such that it will occur with high probability during the duration of the intense ultrashort pulse initiating it. Nuclear

processes can be stimulated in an analogous manner to inelastic scattering in our experiment—by using a precursor molecule (such as HCl) and forcing 're-collision' between a proton and the heavy nucleus with an intense few-cycle optical pulse. To follow the subsequent dynamics, the relative trajectories of the correlated, charged nuclear fragments, as influenced by the field, can be measured.

Regarding the 'probe', we note that any method of observing the relative evolution of the correlated particles can be used for measurement. In molecular science, harmonic generation is one possible method[16] where phase matching eliminates the contribution from all but the first electron wave packet return, which occurs about two-thirds of a period following ionization. Elastic scattering is a second possible method[6], with diffraction determining the nuclear position at the time of re-collision. □

Methods

Production and control of the electron wave packet

An optical parametric amplifier is used to shift the 40-fs output of a Ti:sapphire laser system to longer wavelengths. We use 800 nm, 1.2 μm, 1.53 μm and 1.85 μm pulses. Each ionizes D_2 near the field maximum and provides a progressively longer time delay between ionization and re-collision. Taking the peak of the first electron microbunch to be the delay time, this corresponds to delay times of 1.7, 2.7, 3.4 and 4.2 fs. Changing the wavelength has other implications. The intensity and wavelength determine the maximum re-collision energy $3.17q^2E^2/(4m\omega^2)$ of the electron[7] (q and m are the electron mass and charge, ω and E are the laser pulse's angular frequency and electric field amplitude at the time of ionization). We use a light intensity of 1.5×10^{14} W cm^{-2}, calibrated against the ionization of xenon. Whereas at 800 nm the peak kinetic energy of the re-colliding electron is 30 eV, the ω^{-2} scaling of the kinetic energy means that at 1.85 μm the energy of the peak re-colliding electron is about 160 eV.

Kinetic energy analysis

The kinetic energy spectrum of D^+ was measured with a time-of-flight (TOF) mass spectrometer filled with 10^{-6} torr of D_2. The TOF axis was perpendicular to the direction of propagation of the laser beam. A 1-mm-diameter hole in the electrode placed 1.5 cm from the laser focus selects only those D^+ ions resulting from dissociation of D_2^+ molecules that are aligned along the TOF axis. For the high-resolution results taken with 800-nm light (not shown), the extraction field was 133 V cm^{-1} and the acceptance angle of the TOF was 6 degrees at 8 eV. For the lower-resolution results, the extraction field was 400 V cm^{-1} giving an acceptance angle of 9 degrees at 8 eV.

Selection of the re-collision channel

Deuterium ions are produced by a number of processes during strong field ionization of D_2. We distinguish fragments resulting from inelastic scattering caused by the returning electron (Fig. 2) from those produced by any other process (such as sequential double ionization[22], bond softening[23] and enhanced ionization[24–27]) using the strong sensitivity of recollision phenomena to the ellipticity of the light polarization[6,7,13]. It only takes a small ellipticity to displace the electron laterally with respect to the parent ion so recollision is impossible[7]. In strong fields, the difference between the spectrum obtained with linear and elliptically polarized light is due to recollision.

Received 24 July 2002; accepted 13 January 2003; doi:10.1038/nature01430.

1. Drescher, M. *et al.* Time-resolved atomic inner-shell spectroscopy. *Nature* **419,** 803–807 (2002).
2. Hentschel, M. *et al.* Attosecond metrology. *Nature* **414,** 509–513 (2001).
3. Paul, P. M. *et al.* Observation of a train of attosecond pulses from high harmonic generation. *Science* **292,** 1689–1692 (2001).
4. D'Ariano, G. M., Presti, P. L. & Paris, M. G. A. Using entanglement improves the precision of quantum measurements. *Phys. Rev. Lett.* **87,** 27040 (2001).
5. Resch, K. J., Lundeen, J. S. & Steinberg, A. M. Experimental observation of nonclassical effects on single-photon detection rates. *Phys. Rev. A* **63,** 020102 (2000).
6. Niikura, H. *et al.* Sub-laser-cycle electron pulses for probing molecular dynamics. *Nature* **417,** 917–922 (2002).
7. Corkum, P. B. Plasma perspective on strong field multiphoton ionization. *Phys. Rev. Lett.* **71,** 1994–1997 (1993).
8. Dietrich, P., Burnett, N. H., Ivanov, M. & Corkum, P. B. High harmonic generation and correlated two-electron multiphoton ionization with elliptically polarized light. *Phys. Rev. A* **50,** 3585–3588 (1994).
9. Paulus, G. G., Nicklich, W., Xu, H., Lambropoulos, P. & Walther, H. Plateau in above threshold ionization spectra. *Phys. Rev. Lett.* **72,** 2851–2854 (1994).
10. Weber, Th. *et al.* Correlated electron emission with multiphoton double ionization. *Nature* **405,** 658–661 (2000).
11. Bhardwaj, V. R., Rayner, D. M., Villeneuve, D. M. & Corkum, P. B. Quantum interference in double ionization and fragmentation of C_6H_6 in intense laser fields. *Phys. Rev. Lett.* **87,** 253003 (2001).
12. Zewail, A. H. Femtosecond chemistry. *Science* **242,** 1645–1653 (1988).
13. Krause, J. L., Schafer, K. J. & Kulander, K. C. High-order harmonic generation from atoms and ions in the high intensity regime. *Phys. Rev. Lett.* **68,** 3535–3538 (1992).
14. Lewenstein, M., Balcou, Ph., Ivanov, M. Yu., L'Huillier, A. & Corkum, P. B. Theory of high-harmonic generation by low-frequency laser fields. *Phys. Rev. A* **49,** 2117–2132 (1994).
15. Ivanov, M., Corkum, P. B., Zuo, T. & Bandrauk, A. Routes to control of intense-field atomic polarizability. *Phys. Rev. Lett.* **74,** 2933–2936 (1995).
16. Lein, M., Hay, N., Velotta, R., Marangos, J. P. & Knight, P. L. Role of the intramolecular phase in high-harmonic generation. *Phys. Rev. Lett.* **88,** 183903 (2002).
17. Hargittai, I. & Hargittai, M. *Stereochemical Applications of Gas-Phase Electron Diffraction* (VCH, New York, 1998).
18. Yudin, G. L. & Ivanov, M. Yu. Physics of correlated double ionization of atoms in intense laser fields: Quasistatic tunneling limit. *Phys. Rev. A* **63,** 033404 (2001); erratum **64,** 019902 (2001).
19. Peek, J. M. Inelastic scattering of electrons by the hydrogen molecule ion. *Phys. Rev. A* **134,** 877–883 (1964).
20. Schinke, R. *Photodissociation Dynamics* 114–115 (Cambridge Univ. Press, Cambridge, UK, 1993).
21. Itatani, J. *et al.* Attosecond streak camera. *Phys. Rev. Lett.* **88,** 173903 (2002).
22. Lambropoulos, P. Mechanisms for multiple ionization of atoms by strong pulsed lasers. *Phys. Rev. Lett.* **55,** 2141–2144 (1985).
23. Zavriyev, A., Bucksbaum, P. H., Muller, H. G. & Schumacher, D. W. Ionization and dissociation of H_2 in intense laser fields at 1.064 μm, 532 nm, and 355 nm. *Phys. Rev. A* **42,** R5500–R5513 (1990).
24. Codling, K. & Frasinski, L. J. Dissociative ionization of small molecules in intense laser fields. *J. Phys. B* **26,** 783–809 (1993).
25. Seideman, T., Ivanov, M. Yu. & Corkum, P. B. Role of electron localization in intense-field molecular ionization. *Phys. Rev. Lett.* **75,** 2819–2822 (1995).
26. Zuo, T. & Bandrauk, A. D. Charge-resonance-enhanced ionization of diatomic molecular ions by intense lasers. *Phys Rev. A* **52,** R2511–R2514 (1995).
27. Constant, E., Stapelfeldt, H. & Corkum, P. B. Observation of enhanced ionization of molecular ions in intense laser fields. *Phys. Rev. Lett.* **76,** 4140–4143 (1996).

Acknowledgements We acknowledge discussions with A. Stolow, A. Sokolov, A. D. Bandrauk, S. Chelkowski and J. Marangos. The authors appreciate financial support from Canada's Natural Science and Engineering Research Council, the Canadian Institute for Photonics Innovation, and Le Fonds Québécois de la Recherche sur la Nature et les Technologies.

Competing interests statement The authors declare that they have no competing financial interests.

Correspondence and requests for materials should be addressed to P.B.C. (e-mail: Paul.Corkum@nrc.ca).

Multi-colour organic light-emitting displays by solution processing

C. David Müller*†, Aurélie Falcou‡, Nina Reckefuss*†, Markus Rojahn§, Valèrie Wiederhirn§, Paula Rudati*†, Holger Frohne*†, Oskar Nuyken§, Heinrich Becker‡ & Klaus Meerholz*†

** Department Chemie, Universität München, Butenandtstr. 11, 81377 München, Germany*
‡ Covion Organic Semiconductors GmbH, Industriepark Hoechst, G865, 65926 Frankfurt, Germany
§ Lehrstuhl für Makromolekulare Stoffe, Technische Universität München, Lichtenbergstr. 4, 85747 Garching, Germany

Organic light-emitting diodes (OLEDs) show promise for applications as high-quality self-emissive displays for portable devices such as cellular phones and personal organizers[1–4]. Although monochrome operation is sufficient for some applications, the extension to multi-colour devices—such as RGB (red, green, blue) matrix displays—could greatly enhance their technological impact. Multi-colour OLEDs have been successfully fabricated by vacuum deposition of small electroluminescent molecules, but solution processing of larger molecules (electroluminescent polymers) would result in a cheaper and simpler manufacturing process. However, it has proved difficult to combine the solution processing approach with the high-resolution patterning techniques required to produce a pixelated display. Recent attempts have focused on the modification of standard printing techniques, such as screen printing[5–7] and ink jetting[8], but those still have technical drawbacks. Here we report a class of electroluminescent polymers that can be patterned in a way similar to standard photoresist materials—soluble polymers with oxetane

† Present address: Institut für Physikalische Chemie, Universität zu Köln, Luxemburgerstr. 116, 50939 Köln, Germany.